Upper limits from the LIGO and TAMA detectors on the rate of gravitational-wave bursts

B. Abbott,[1] R. Abbott,[1] R. Adhikari,[1] A. Ageev,[2,3] J. Agresti,[1] P. Ajith,[4] B. Allen,[5] J. Allen,[6] R. Amin,[7] S. B. Anderson,[1] W. G. Anderson,[8] M. Araya,[1] H. Armandula,[1] M. Ashley,[9] F. Asiri,[1,a] P. Aufmuth,[10] C. Aulbert,[11] S. Babak,[12] R. Balasubramanian,[12] S. Ballmer,[6] B. C. Barish,[1] C. Barker,[13] D. Barker,[13] M. Barnes,[1,b] B. Barr,[14] M. A. Barton,[1] K. Bayer,[6] R. Beausoleil,[15,c] K. Belczynski,[16] R. Bennett,[14,d] S. J. Berukoff,[11,e] J. Betzwieser,[6] B. Bhawal,[1] I. A. Bilenko,[2] G. Billingsley,[1] E. Black,[1] K. Blackburn,[1] L. Blackburn,[6] B. Bland,[13] B. Bochner,[6,f] L. Bogue,[17] R. Bork,[1] S. Bose,[18] P. R. Brady,[5] V. B. Braginsky,[2] J. E. Brau,[19] D. A. Brown,[1] A. Bullington,[15] A. Bunkowski,[4,10] A. Buonanno,[20] R. Burgess,[6] D. Busby,[1] W. E. Butler,[21] R. L. Byer,[15] L. Cadonati,[6] G. Cagnoli,[14] J. B. Camp,[22] J. Cannizzo,[22] K. Cannon,[5] C. A. Cantley,[14] J. Cao,[6] L. Cardenas,[1] K. Carter,[17] M. M. Casey,[14] J. Castiglione,[23] A. Chandler,[1] J. Chapsky,[1,b] P. Charlton,[1,g] S. Chatterji,[1] S. Chelkowski,[4,10] Y. Chen,[11] V. Chickarmane,[7,h] D. Chin,[24] N. Christensen,[25] D. Churches,[12] T. Cokelaer,[12] C. Colacino,[26] R. Coldwell,[23] M. Coles,[17,i] D. Cook,[13] T. Corbitt,[6] D. Coyne,[1] J. D. E. Creighton,[5] T. D. Creighton,[1] D. R. M. Crooks,[14] P. Csatorday,[6] B. J. Cusack,[27] C. Cutler,[11] J. Dalrymple,[3] E. D'Ambrosio,[1] K. Danzmann,[4,10] G. Davies,[12] E. Daw,[7,j] D. DeBra,[15] T. Delker,[23,k] V. Dergachev,[24] S. Desai,[9] R. DeSalvo,[1] S. Dhurandhar,[28] A. Di Credico,[3] M. Díaz,[8] H. Ding,[1] R. W. P. Drever,[29] R. J. Dupuis,[1] J. A. Edlund,[1,b] P. Ehrens,[1] E. J. Elliffe,[14] T. Etzel,[1] M. Evans,[1] T. Evans,[17] S. Fairhurst,[5] C. Fallnich,[10] D. Farnham,[1] M. M. Fejer,[15] T. Findley,[30] M. Fine,[1] L. S. Finn,[9] K. Y. Franzen,[23] A. Freise,[4,l] R. Frey,[19] P. Fritschel,[6] V. V. Frolov,[17] M. Fyffe,[17] K. S. Ganezer,[31] J. Garofoli,[13] J. A. Giaime,[7] A. Gillespie,[1,m] K. Goda,[6] L. Goggin,[1] G. González,[7] S. Goßler,[10] P. Grandclément,[16,n] A. Grant,[14] C. Gray,[13] A. M. Gretarsson,[32] D. Grimmett,[1] H. Grote,[4] S. Grunewald,[11] M. Guenther,[13] E. Gustafson,[15,o] R. Gustafson,[24] W. O. Hamilton,[7] M. Hammond,[17] C. Hanna,[7] J. Hanson,[17] C. Hardham,[15] J. Harms,[33] G. Harry,[6] A. Hartunian,[1] J. Heefner,[1] Y. Hefetz,[6] G. Heinzel,[4] I. S. Heng,[10] M. Hennessy,[15] N. Hepler,[9] A. Heptonstall,[14] M. Heurs,[10] M. Hewitson,[4] S. Hild,[4] N. Hindman,[13] P. Hoang,[1] J. Hough,[14] M. Hrynevych,[1,p] W. Hua,[15] M. Ito,[19] Y. Itoh,[11] A. Ivanov,[1] O. Jennrich,[14,q] B. Johnson,[13] W. W. Johnson,[7] W. R. Johnston,[8] D. I. Jones,[9] G. Jones,[12] L. Jones,[1] D. Jungwirth,[1,r] V. Kalogera,[16] E. Katsavounidis,[6] K. Kawabe,[13] W. Kells,[1] J. Kern,[17,s] A. Khan,[17] S. Killbourn,[14] C. J. Killow,[14] C. Kim,[16] C. King,[1] P. King,[1] S. Klimenko,[23] S. Koranda,[5] K. Kötter,[10] J. Kovalik,[17,b] D. Kozak,[1] B. Krishnan,[11] M. Landry,[13] J. Langdale,[17] B. Lantz,[15] R. Lawrence,[6] A. Lazzarini,[1] M. Lei,[1] I. Leonor,[19] K. Libbrecht,[1] A. Libson,[25] P. Lindquist,[1] S. Liu,[1] J. Logan,[1,t] M. Lormand,[17] M. Lubinski,[13] H. Lück,[4,10] M. Luna,[34] T. T. Lyons,[1,t] B. Machenschalk,[11] M. MacInnis,[6] M. Mageswaran,[1] K. Mailand,[1] W. Majid,[1,b] M. Malec,[4,10] V. Mandic,[1] F. Mann,[1] A. Marin,[6,u] S. Márka,[35] E. Maros,[1] J. Mason,[1,v] K. Mason,[6] O. Matherny,[13] L. Matone,[35] N. Mavalvala,[6] R. McCarthy,[13] D. E. McClelland,[27] M. McHugh,[36] J. W. C. McNabb,[9] A. Melissinos,[21] G. Mendell,[13] R. A. Mercer,[26] S. Meshkov,[1] E. Messaritaki,[5] C. Messenger,[26] E. Mikhailov,[6] S. Mitra,[28] V. P. Mitrofanov,[2] G. Mitselmakher,[23] R. Mittleman,[6] O. Miyakawa,[1] S. Mohanty,[8] G. Moreno,[13] K. Mossavi,[4] G. Mueller,[23] S. Mukherjee,[8] P. Murray,[14] E. Myers,[37] J. Myers,[13] S. Nagano,[4] T. Nash,[1] R. Nayak,[28] G. Newton,[14] F. Nocera,[1] J. S. Noel,[18] P. Nutzman,[16] T. Olson,[38] B. O'Reilly,[17] D. J. Ottaway,[6] A. Ottewill,[5,w] D. Ouimette,[1,r] H. Overmier,[17] B. J. Owen,[9] Y. Pan,[39] M. A. Papa,[11] V. Parameshwaraiah,[13] C. Parameswariah,[17] M. Pedraza,[1] S. Penn,[40] M. Pitkin,[14] M. Plissi,[14] R. Prix,[11] V. Quetschke,[23] F. Raab,[13] H. Radkins,[13] R. Rahkola,[11] M. Rakhmanov,[23] S. R. Rao,[1] K. Rawlins,[6,x] S. Ray-Majumder,[5] V. Re,[26] D. Redding,[1,b] M. W. Regehr,[1,b] T. Regimbau,[12] S. Reid,[14] K. T. Reilly,[1] K. Reithmaier,[1] D. H. Reitze,[23] S. Richman,[6,y] R. Riesen,[17] K. Riles,[24] B. Rivera,[13] A. Rizzi,[17,z] D. I. Robertson,[14] N. A. Robertson,[14,15] C. Robinson,[12] L. Robison,[1] S. Roddy,[17] A. Rodriguez,[7] J. Rollins,[35] J. D. Romano,[12] J. Romie,[1] H. Rong,[23,m] D. Rose,[1] E. Rotthoff,[9] S. Rowan,[14] A. Rüdiger,[4] L. Ruet,[6] P. Russell,[1] K. Ryan,[13] I. Salzman,[1] V. Sandberg,[13] G. H. Sanders,[1,aa] V. Sannibale,[1] P. Sarin,[6] B. Sathyaprakash,[12] P. R. Saulson,[23] R. Savage,[13] A. Sazonov,[23] R. Schilling,[4] K. Schlaufman,[9] V. Schmidt,[1,ab] R. Schnabel,[33] R. Schofield,[19] B. F. Schutz,[11,12] P. Schwinberg,[13] S. M. Scott,[27] S. E. Seader,[18] A. C. Searle,[27] B. Sears,[1] S. Seel,[1] F. Seifert,[33] D. Sellers,[17] A. S. Sengupta,[28] C. A. Shapiro,[9,ac] P. Shawhan,[1] D. H. Shoemaker,[6] Q. Z. Shu,[23,ad] A. Sibley,[17] X. Siemens,[5] L. Sievers,[1,b] D. Sigg,[13] A. M. Sintes,[11,34] J. R. Smith,[4] M. Smith,[6] M. R. Smith,[1] P. H. Sneddon,[14] R. Spero,[1,b] O. Spjeld,[17] G. Stapfer,[17] D. Steussy,[25] K. A. Strain,[14] D. Strom,[19] A. Stuver,[9] T. Summerscales,[9] M. C. Sumner,[1] M. Sung,[7] P. J. Sutton,[1] J. Sylvestre,[1,ae] D. B. Tanner,[23] H. Tariq,[1] M. Tarallo,[1] I. Taylor,[12] R. Taylor,[14] R. Taylor,[1] K. A. Thorne,[9] K. S. Thorne,[39] M. Tibbits,[9] S. Tilav,[1,af] M. Tinto,[29,b] K. V. Tokmakov,[2] C. Torres,[8] C. Torrie,[1] G. Traylor,[17] W. Tyler,[1] D. Ugolini,[41] C. Ungarelli,[26] M. Vallisneri,[39,ag] M. van Putten,[6] S. Vass,[1] A. Vecchio,[26] J. Veitch,[14] C. Vorvick,[13] S. P. Vyachanin,[2] L. Wallace,[1] H. Walther,[33] H. Ward,[14] R. Ward,[1] B. Ware,[1,b] K. Watts,[17] D. Webber,[1] A. Weidner,[33,4] U. Weiland,[10] A. Weinstein,[1] R. Weiss,[6] H. Welling,[10] L. Wen,[11] S. Wen,[7] K. Wette,[27] J. T. Whelan,[36] S. E. Whitcomb,[1] B. F. Whiting,[23] S. Wiley,[31] C. Wilkinson,[13] P. A. Willems,[1] P. R. Williams,[11,ah] R. Williams,[29] B. Willke,[4,10] A. Wilson,[1] B. J. Winjum,[9,e]

W. Winkler,[4] S. Wise,[23] A. G. Wiseman,[5] G. Woan,[14] D. Woods,[5] R. Wooley,[17] J. Worden,[13] W. Wu,[23] I. Yakushin,[17]
H. Yamamoto,[1] S. Yoshida,[30] K. D. Zaleski,[9] M. Zanolin,[6] I. Zawischa,[10,ai] L. Zhang,[1] R. Zhu,[11] N. Zotov,[42]
M. Zucker,[17] and J. Zweizig[1]

(LIGO Scientific Collaboration)[aj]

[1]*LIGO–California Institute of Technology, Pasadena, California 91125, USA*
[2]*Moscow State University, Moscow, 119992, Russia*
[3]*Syracuse University, Syracuse, New York 13244, USA*
[4]*Albert-Einstein-Institut, Max-Planck-Institut für Gravitationsphysik, D-30167 Hannover, Germany*
[5]*University of Wisconsin-Milwaukee, Milwaukee, Wisconsin 53201, USA*
[6]*LIGO–Massachusetts Institute of Technology, Cambridge, Massachusetts 02139, USA*
[7]*Louisiana State University, Baton Rouge, Louisiana 70803, USA*
[8]*The University of Texas at Brownsville, Brownsville, Texas 78520, USA*
and Texas Southmost College, Brownsville, Texas 78520, USA
[9]*The Pennsylvania State University, University Park, Pennsylvania 16802, USA*
[10]*Universität Hannover, D-30167 Hannover, Germany*
[11]*Albert-Einstein-Institut, Max-Planck-Institut für Gravitationsphysik, D-14476 Golm, Germany*
[12]*Cardiff University, Cardiff, CF2 3YB, United Kingdom*
[13]*LIGO Hanford Observatory, Richland, Washington 99352, USA*
[14]*University of Glasgow, Glasgow, G12 8QQ, United Kingdom*
[15]*Stanford University, Stanford, California 94305, USA*
[16]*Northwestern University, Evanston, Illinois 60208, USA*
[17]*LIGO Livingston Observatory, Livingston, Louisiana 70754, USA*
[18]*Washington State University, Pullman, Washington 99164, USA*
[19]*University of Oregon, Eugene, Oregon 97403, USA*
[20]*University of Maryland, College Park, Maryland 20742 USA*
[21]*University of Rochester, Rochester, New York 14627, USA*
[22]*NASA/Goddard Space Flight Center, Greenbelt, Maryland 20771, USA*
[23]*University of Florida, Gainesville, Florida 32611, USA*
[24]*University of Michigan, Ann Arbor, Michigan 48109, USA*
[25]*Carleton College, Northfield, Minnesota 55057, USA*
[26]*University of Birmingham, Birmingham, B15 2TT, United Kingdom*
[27]*Australian National University, Canberra, 0200, Australia*
[28]*Inter-University Centre for Astronomy and Astrophysics, Pune - 411007, India*
[29]*California Institute of Technology, Pasadena, California 91125, USA*
[30]*Southeastern Louisiana University, Hammond, Louisiana 70402, USA*
[31]*California State University Dominguez Hills, Carson, California 90747, USA*
[32]*Embry-Riddle Aeronautical University, Prescott, Arizona 86301 USA*
[33]*Max Planck Institut für Quantenoptik, D-85748, Garching, Germany*
[34]*Universitat de les Illes Balears, E-07122 Palma de Mallorca, Spain*
[35]*Columbia University, New York, New York 10027, USA*
[36]*Loyola University, New Orleans, Louisiana 70118, USA*
[37]*Vassar College, Poughkeepsie, New York 12604, USA*
[38]*Salish Kootenai College, Pablo, Montana 59855, USA*
[39]*Caltech-CaRT, Pasadena, California 91125, USA*
[40]*Hobart and William Smith Colleges, Geneva, New York 14456, USA*
[41]*Trinity University, San Antonio, Texas 78212, USA*
[42]*Louisiana Tech University, Ruston, Louisiana 71272, USA*

T. Akutsu,[43] T. Akutsu,[44] M. Ando,[45] K. Arai,[46] A. Araya,[47] H. Asada,[48] Y. Aso,[45] P. Beyersdorf,[46] Y. Fujiki,[49]
M.-K. Fujimoto,[46] R. Fujita,[50] M. Fukushima,[46] T. Futamase,[51] Y. Hamuro,[49] T. Haruyama,[52] K. Hayama,[46] H. Iguchi,[53]
Y. Iida,[45] K. Ioka,[57] H. Ishizuka,[43] N. Kamikubota,[52] N. Kanda,[54] T. Kaneyama,[49] Y. Karasawa,[51] K. Kasahara,[43]
T. Kasai,[48] M. Katsuki,[54] S. Kawamura,[46] M. Kawamura,[49] F. Kawazoe,[55] Y. Kojima,[56] K. Kokeyama,[55] K. Kondo,[43]
Y. Kozai,[46] H. Kudoh,[45] K. Kuroda,[43] T. Kuwabara,[49] N. Matsuda,[58] N. Mio,[59] K. Miura,[60] S. Miyama,[46] S. Miyoki,[43]
H. Mizusawa,[49] S. Moriwaki,[59] M. Musha,[61] Y. Nagayama,[54] K. Nakagawa,[61] T. Nakamura,[57] H. Nakano,[54] K. Nakao,[54]
Y. Nishi,[45] K. Numata,[45] Y. Ogawa,[52] M. Ohashi,[43] N. Ohishi,[46] A. Okutomi,[43] K. Oohara,[49] S. Otsuka,[45] Y. Saito,[52]
S. Sakata,[55] M. Sasaki,[66] N. Sato,[52] S. Sato,[46] Y. Sato,[61] K. Sato,[62] A. Sekido,[63] N. Seto,[50] M. Shibata,[64] H. Shinkai,[65]

T. Shintomi,[52] K. Soida,[45] K. Somiya,[59] T. Suzuki,[52] H. Tagoshi,[50] H. Takahashi,[49] R. Takahashi,[46] A. Takamori,[47] S. Takemoto,[57] K. Takeno,[59] T. Tanaka,[66] K. Taniguchi,[69] T. Tanji,[59] D. Tatsumi,[46] S. Telada,[68] M. Tokunari,[43] T. Tomaru,[52] K. Tsubono,[45] N. Tsuda,[62] Y. Tsunesada,[46] T. Uchiyama,[43] K. Ueda,[61] A. Ueda,[46] K. Waseda,[46] A. Yamamoto,[52] K. Yamamoto,[43] T. Yamazaki,[46] Y. Yanagi,[55] J. Yokoyama,[67] T. Yoshida,[51] and Z.-H. Zhu[46]

(TAMA Collaboration)

[43]*Institute for Cosmic Ray Research, The University of Tokyo, Kashiwa, Chiba 277-8582, Japan*
[44]*Department of Astronomy, The University of Tokyo, Bunkyo-ku, Tokyo 113-0033, Japan*
[45]*Department of Physics, The University of Tokyo, Bunkyo-ku, Tokyo 113-0033, Japan*
[46]*National Astronomical Observatory of Japan, Tokyo 181-8588, Japan*
[47]*Earthquake Research Institute, The University of Tokyo, Bunkyo-ku, Tokyo 113-0032, Japan*
[48]*Faculty of Science and Technology, Hirosaki University, Hirosaki, Aomori 036-8561, Japan*
[49]*Faculty of Science, Niigata University, Niigata, Niigata 950-2102, Japan*
[50]*Graduate School of Science, Osaka University, Toyonaka, Osaka 560-0043, Japan*
[51]*Graduate School of Science, Tohoku University, Sendai, Miyagi 980-8578, Japan*
[52]*High Energy Accelerator Research Organization, Tsukuba, Ibaraki 305-0801, Japan*
[53]*Tokyo Institute of Technology, Meguro-ku, Tokyo 152-8551, Japan*
[54]*Graduate School of Science, Osaka City University, Sumiyoshi-ku, Osaka 558-8585, Japan*
[55]*Ochanomizu University, Bunkyo-ku, Tokyo 112-8610, Japan*
[56]*Department of Physics, Hiroshima University, Higashi-Hiroshima, Hiroshima 739-8526, Japan*
[57]*Faculty of Science, Kyoto University, Sakyo-ku, Kyoto 606-8502, Japan*
[58]*Tokyo Denki University, Chiyoda-ku, Tokyo 101-8457, Japan*
[59]*Department of Advanced Materials Science, The University of Tokyo, Kashiwa, Chiba 277-8561, Japan*
[60]*Department of Physics, Miyagi University of Education, Aoba Aramaki, Sendai 980-0845, Japan*
[61]*Institute for Laser Science, University of Electro-Communications, Chofugaoka, Chofu, Tokyo 182-8585, Japan*
[62]*Precision Engineering Division, Faculty of Engineering, Tokai University, Hiratsuka, Kanagawa 259-1292, Japan*
[63]*Waseda University, Shinjyuku-ku, Tokyo 169-8555, Japan*
[64]*Graduate School of Arts and Sciences, The University of Tokyo, Meguro-ku, Tokyo 153-8902, Japan*
[65]*RIKEN, Wako, Saitaka 351-0198, Japan*
[66]*Yukawa Institute for Theoretical Physics, Kyoto University, Sakyo-ku, Kyoto 606-8502, Japan*
[67]*Research Center for the Early Universe (RESCEU), Graduate School of Science, The University of Tokyo, Tokyo 113-0033, Japan*
[68]*National Institute of Advanced Industrial Science and Technology, Tsukuba, Ibaraki 305-8563, Japan*
[69]*Department of Physics, University of Illinois at Urbana-Champaign, Urbana, IL 61801, USA*

We report on the first joint search for gravitational waves by the TAMA and LIGO collaborations. We looked for millisecond-duration unmodeled gravitational-wave bursts in 473 hr of coincident data collected during early 2003. No candidate signals were found. We set an upper limit of 0.12 events per day on the rate of detectable gravitational-wave bursts, at 90% confidence level. From software

---

[a]Currently at Stanford Linear Accelerator Center
[b]Currently at Jet Propulsion Laboratory.
[c]Permanent address: HP Laboratories.
[d]Currently at Rutherford Appleton Laboratory.
[e]Currently at University of CA, Los Angeles.
[f]Currently at Hofstra University.
[g]Currently at Charles Sturt University, Australia.
[h]Currently at Keck Graduate Institute.
[i]Currently at National Science Foundation.
[j]Currently at University of Sheffield.
[k]Currently at Ball Aerospace Corporation.
[l]Currently at European Gravitational Observatory.
[m]Currently at Intel Corp.
[n]Currently at University of Tours, France.
[o]Currently at Lightconnect Inc.
[p]Currently at W.M. Keck Observatory.
[q]Currently at ESA Science and Technology Center.
[r]Currently at Raytheon Corporation.
[s]Currently at NM Institute of Mining and Technology / Magdalena Ridge Observatory Interferometer.

[t]Currently at Mission Research Corporation.
[u]Currently at Harvard University.
[v]Currently at Lockheed-Martin Corporation.
[w]Permanent address: University College Dublin.
[x]Currently at University of AK Anchorage.
[y]Currently at Research Electro-Optics Inc.
[z]Currently at Institute of Advanced Physics, Baton Rouge, LA.
[aa]Currently at Thirty Meter Telescope Project at Caltech.
[bb]Currently at European Commission, DG Research, Brussels, Belgium.
[cc]Currently at University of Chicago.
[dd]Currently at LightBit Corporation.
[ee]Permanent address: IBM Canada Ltd.
[ff]Currently at University of DE.
[gg]Permanent address: Jet Propulsion Laboratory.
[hh]Currently at Shanghai Astronomical Observatory.
[ii]Currently at Laser Zentrum Hannover.
[jj]Electronic address: http://www.ligo.org

simulations, we estimate that our detector network was sensitive to bursts with root-sum-square strain amplitude above approximately $1-3 \times 10^{-19}$ Hz$^{-1/2}$ in the frequency band 700-2000 Hz. We describe the details of this collaborative search, with particular emphasis on its advantages and disadvantages compared to searches by LIGO and TAMA separately using the same data. Benefits include a lower background and longer observation time, at some cost in sensitivity and bandwidth. We also demonstrate techniques for performing coincidence searches with a heterogeneous network of detectors with different noise spectra and orientations. These techniques include using coordinated software signal injections to estimate the network sensitivity, and tuning the analysis to maximize the sensitivity and the livetime, subject to constraints on the background.

I. INTRODUCTION

At present several large-scale interferometric gravitational-wave detectors are operating or are being commissioned: GEO [1], LIGO [2], TAMA [3], and Virgo [4]. In addition, numerous resonant-mass detectors have been operating for a number of years [5–7]. Cooperative analyses by these observatories could be valuable for making confident detections of gravitational waves and for extracting maximal information from them. This is particularly true for gravitational-wave bursts (GWBs) from systems such as core-collapse supernovae [8–11], black-hole mergers [12,13], and gamma-ray bursters [14], for which we have limited theoretical knowledge of the source and the resulting gravitational waveform to guide us. Advantages of coincident observations include a decreased background from random detector noise fluctuations, an increase in the total observation time during which some minimum number of detectors are operating, and the possibility of locating a source on the sky and extracting polarization information (when detectors at three or more sites observe a signal) [15]. Independent observations using different detector hardware and software also decrease the possibility of error or bias.

There are also disadvantages to joint searches. Most notably, in a straightforward coincidence analysis the sensitivity of a network is limited by the least sensitive detector. In addition, differences in alignment mean that different detectors will be sensitive to different combinations of the two polarization components of a gravitational wave. This complicates attempts to compare the signal amplitude or waveform as measured by different detectors. Finally, differences in hardware, software, and algorithms make collaborative analyses technically challenging.

In this article we present the first observational results from a joint search for gravitational waves by the LIGO and TAMA collaborations. We perform a coincidence analysis targeting generic millisecond-duration GWBs, requiring candidate GWBs to be detected by all operating LIGO and TAMA interferometers. This effort is complementary to searches for GWBs performed independently by LIGO [16] and TAMA [17] using the same data that we analyze here. Our goal is to highlight the strengths and weaknesses of our joint search relative to these single-collaboration searches, and to demonstrate techniques for performing coincidence searches with a heterogeneous network of detectors with different noise spectra and orientations. This search could form a prototype for more comprehensive collaborative analyses in the future.

In Sec. II we review the performance of the LIGO and TAMA detectors during the joint observations used for this search. We describe the analysis procedure in Sec. III, and the tuning of the analysis in Sec. IV. The results of the search are presented in Sec. V. We conclude with some brief comments in Sec. VI.

II. LIGO-TAMA NETWORK AND DATA SETS

The LIGO network consists of a 4 km interferometer "L1" near Livingston, Louisiana and 4 km "H1" and 2 km "H2" interferometers which share a common vacuum system on the Hanford site in Washington. The TAMA group operates a 300 m interferometer "T1" near Tokyo. These instruments attempt to detect gravitational waves by monitoring the interference of the laser light from each of two perpendicular arms. Minute differential changes in the arm lengths produced by a passing gravitational wave alter this interference pattern. Basic information on the position and orientation of the LIGO and TAMA detectors can be found in [18,19]. Detailed descriptions of their operation can be found in [2,16,17,20].

In a search for gravitational-wave bursts, the key characteristics of a detector are the orientation, the noise spectrum and its variability, and the observation time.

The response of an interferometer to a gravitational wave depends on the relative orientation of the source and the detector, as well as on the signal polarization. Figure 1 shows the variation in the polarization-averaged sensitivities of the LIGO and TAMA detectors as a function of the sky position of the source. It is clear from these figures that LIGO and TAMA have maximum sensitivity to different portions of the sky. This complicates a search based on coincident detections: there is a loss of sensitivity to weak signals; and it is difficult to compare quantitatively the signal amplitude or waveform as measured by the LIGO and TAMA detectors since they will not, in general, be the same. (This was not a significant problem in previous multidetector searches by LIGO [16,21] and the IGEC [7], since they employed approximately coaligned detectors.) We account for these effects by using coordi-
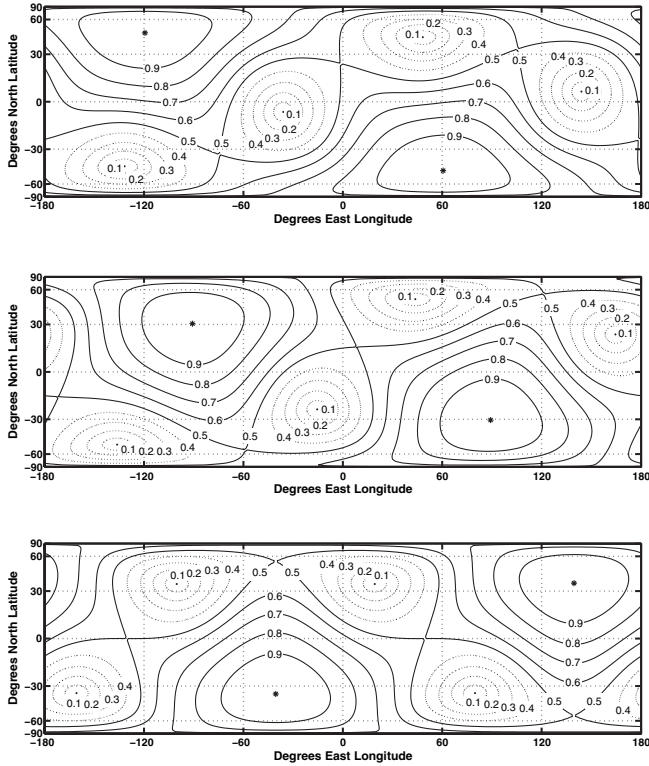
FIG. 1.   Polarization-averaged antenna amplitude responses $(F_+^2 + F_\times^2)^{1/2} \in [0, 1]$, in Earth-based coordinates. [See Eq. (4.3) and [19] for definitions of these functions and of Earth-based coordinates.] The top plot is for the LIGO Hanford detectors (H1, H2). The middle plot is for LIGO Livingston (L1). The bottom plot is for TAMA (T1). High contour values indicate sky directions of high sensitivity. The directions of maximum (null) sensitivity for each detector are indicated by the * (.) symbols. The directions of LIGO's maximum sensitivity lie close to areas of TAMA's worst sensitivity and vice versa.

nated simulations to guide the tuning of our analysis so as to maximize the detection efficiency of the network, and we forego amplitude and waveform consistency tests between LIGO and TAMA; see Secs. III and IV.

The data analyzed in this search were collected during the LIGO science run 2 (S2) and the TAMA data taking run 8 (DT8), between 14 February 2003 and 14 April 2003. Figures 2 and 3 show representative strain noise spectra from each detector during S2/DT8. Ignoring differences in antenna response, requiring coincident detection of a candidate signal by both LIGO and TAMA means that the sensitivity of the network will be limited by the least sensitive detector. This motivates concentrating our efforts on the frequency band where all detectors have comparable sensitivity; i.e., near the minimum of the noise envelope. Specifically, we choose to search for GWBs that have significant power in the frequency range 700-2000 Hz. Restricting the frequency range in this manner reduces the background due to coincident noise fluctuations, while
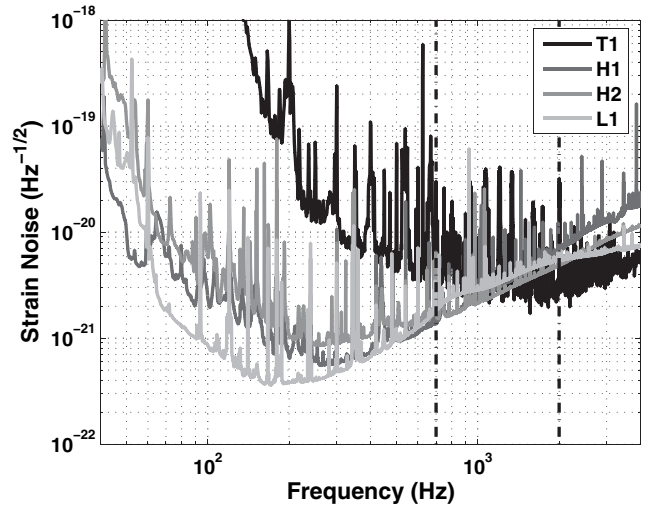

FIG. 2.   S2-averaged amplitude noise spectra for the LIGO detectors, and a representative DT8 spectrum for the TAMA detector. We focus on GWBs which have significant energy in the frequency range 700-2000 Hz (indicated by the vertical dashed lines), where each interferometer has approximately the same noise level.

preserving the sensitivity of the network to GWBs that are detectable by both LIGO and TAMA. Note also that the LIGO collaboration has carried out an independent GWB analysis of the S2 data concentrating on the band 100-1100 Hz [16]. There is thus no danger in missing a real detectable burst which might have occurred at lower frequencies,
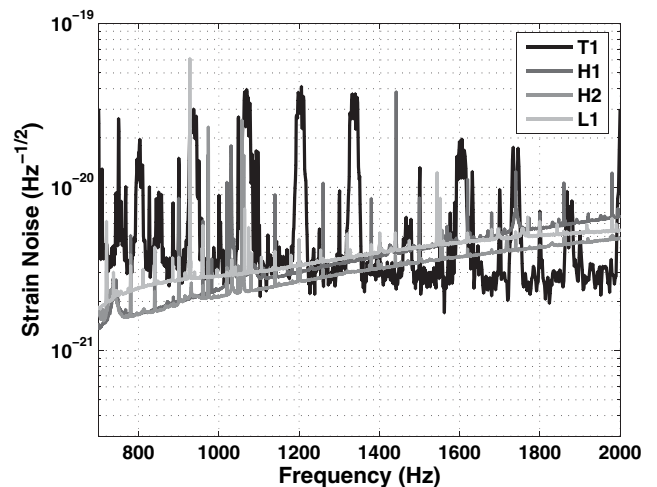

FIG. 3.   The same amplitude noise spectra as in Fig. 2, focusing on the frequency range 700-2000 Hz. The peaks at multiples of 400/3 Hz in the TAMA spectrum are due to a coupling between the radio-frequency modulation signal and the laser source; these frequencies are removed by the data conditioning discussed in Sec. III A 2.

TABLE I.   Observation times and duty cycles of the LIGO and TAMA detectors individually, and in various combinations, during S2/DT8. The symbol nL1 (nT1) indicates times when L1 (T1) was not operating. The network data sets are disjoint (nonoverlapping).

Detector combination	Observation time (hr)	Fraction of total observation time
H1	1040	74%
H2	821	58%
L1	536	38%
T1	1158	82%
H1-H2-L1-T1	256	18%
H1-H2-nL1-T1	320	23%
H1-H2-L1-nT1	62	4%
network totals	638	45%

since it should have been detected by this complementary search.

Table I shows the amount of time in S2/DT8 during which each detector was operating. As we shall see in Sec. IV B, the LIGO-TAMA network achieved its lowest background rate during periods when both of the LIGO Hanford interferometers (H1 and H2) and at least one of the LIGO Livingston and TAMA interferometers (L1 and T1) were operating. Restricting our analysis to these detector combinations gives us three independent data sets: the quadruple-coincidence data set, denoted H1-H2-L1-T1; the data set during which L1 was not operating, denoted H1-H2-nL1-T1, and the data set during which T1 was not operating, denoted H1-H2-L1-nT1 ("n" for "not operating"). The observation time for each of these data sets is also shown in Table I.

The LIGO-TAMA quadruple-coincidence data set (H1-H2-L1-T1) is particularly well-suited to making confident detections of gravitational-wave bursts, since combining so many detectors naturally suppresses the background from accidental coincidences—to well below one per year, in our case—while maintaining high detection sensitivity. Meanwhile, the triple-coincidence data sets (H1-H2-nL1-T1 and H1-H2-L1-nT1) contribute the bulk of our observation time. In particular, the high T1 duty cycle (82%) allows us to use the large amount of H1-H2 data in H1-H2-nL1-T1 coincidence that would otherwise be discarded because of the poor L1 duty cycle (33%). The LIGO-TAMA detector network therefore has more than twice as much useful data as the LIGO detectors alone. This increase in observation time allows a proportional decrease in the limit on the GWB rate which we are able to set with the combined detector network (for negligible background), and increases the probability of seeing a rare strong gravitational-wave event. Furthermore, while the LIGO-TAMA network uses only half of the TAMA data, we shall see that the suppression of the background by coincidence allows it to place stronger upper limits on weak GWBs than can TAMA alone.

The LIGO and TAMA detectors had not yet reached their design sensitivities by the time of the S2/DT8 run;

nevertheless, the quantity of coincident data available—nearly 600 hours—provided an excellent opportunity to develop and test joint searches between our collaborations. In addition, the amplitude spectral density of the strain noise of these instruments in their common frequency band was comparable to resonant-mass detectors [7,22]. Thus, the interferometers, with their much broader bandwidth, had better sensitivity to broadband signals; see [16] for a direct comparison.

III. ANALYSIS METHOD

Our analysis methodology is similar, though not identical, to that used in the LIGO S1 and S2 untriggered GWB searches [16,21]. The essential steps are illustrated in Fig. 4. These are:

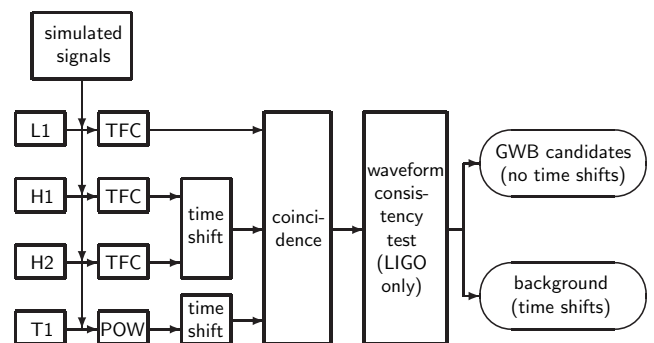(1) Search the data from each detector separately for burst events.

FIG. 4.   Schematic of our analysis pipeline. Data from each detector is analyzed for bursts using the TFCLUSTERS (TFC) or EXCESS POWER (POW) algorithm. Optionally, a time shift of 5–115 s is added to the event triggers from some sites. We look for simultaneous events from each operating detector, then apply the r-statistic waveform consistency test to the data from the LIGO detectors. Surviving coincidences are possible GWBs if no time shifts were used; otherwise they are accidental coincidences (background). The detection efficiency of the network is estimated by adding simulated GWBs to the data from each detector and repeating the analysis. Note that one of the L1 or T1 detectors may not be operating at any given time.

(2) Look for simultaneous ("coincident") events in all operating detectors.

(3) Perform a waveform consistency test on the data from the LIGO interferometers around the time of each coincidence.

(4) Estimate the background rate from coincident detector noise fluctuations by repeating the coincidence and waveform consistency tests after artificially shifting in time the events from different sites.

(5) Compare the number of coincidences without time shifts to that expected from the background to set an upper limit on the rate of detectable bursts. (A significant excess of events indicates a possible detection.)

(6) Estimate the network sensitivity to true GWBs (i.e., the false dismissal probability) by adding simulated signals to the detector data and repeating the analysis.

In the following subsections we describe these steps in more detail. In addition, the various thresholds used for event generation, coincidence, etc., are tuned to maximize the sensitivity of the analysis; this tuning is described in Sec. IV B.

The LIGO software used in this analysis is available publicly [23].

A. Event trigger generation

To maintain sensitivity to the widest range of signals, our burst-detection algorithms do not use templates. Instead, they look for transient excesses of power in the detector output. The production of lists of transient events, or *event triggers*, was done independently by LIGO and TAMA, using different algorithms. Since both of the algorithms used have been described elsewhere, we review them only briefly.

1. TFCLUSTERS

The LIGO triggers were produced using the TFCLUSTERS burst-detection algorithm [21,24].

Before processing in TFCLUSTERS, the data from a given detector are first high-pass filtered and whitened using a linear predictor error filter [25,26]. The TFCLUSTERS algorithm then constructs a time-frequency spectrogram of the filtered data by segmenting the data into 50% overlapping time intervals and Fourier transforming. The fraction p of highest-power pixels in each frequency bin are selected as *black* pixels, where p is the *black pixel probability*. (Note that this thresholding is inherently adaptive, so that the rate of triggers is not unduly affected by slow trends in the noise floor.) Event triggers are formed from clusters of nearest-neighbor black pixels that exceed a specified size. In keeping with our choice of frequency band, only triggers that overlap 700-2000 Hz are retained; all others are discarded. These triggers are then passed to a function which makes

refined estimates of their peak time, duration, central frequency, and bandwidth.

2. EXCESS POWER

The TAMA triggers used in this joint analysis were generated in a TAMA-only search for GWBs [17] using an EXCESS POWER algorithm. The event generation was therefore not tuned specifically for a LIGO-TAMA coincidence analysis.

The TAMA data are first conditioned to remove lines (including the peaks at multiples of 400/3 Hz visible in Fig. 3). It is then divided into 87.5% overlapping segments and Fourier transformed. The resulting spectrogram is normalized by the background estimated over the previous 30 min. (This fixed averaging time was chosen for convenience, although examination of TAMA event triggers indicates that the noise background was not always stationary on this time scale.) The signal-to-noise ratio (SNR) is then summed over a fixed set of frequency bins in the range 230-2500 Hz, and a trigger produced when the SNR exceeds the threshold $\rho_0 = 4$. Triggers separated by less than 25 ms are reported as a single event characterized by the peak time, duration (time above threshold), and SNR. Because of the use of a frequency mask, no frequency information is assigned to the trigger. Finally, triggers occurring simultaneously with excursions in the intensity of the light in the recycling cavity are vetoed (ignored), as are triggers that fail a time-scale test designed to pass only millisecond-duration events [17].

While the TAMA triggers range over 230-2500 Hz, the LIGO triggers were required to overlap 700-2000 Hz. Since a GWB with frequency content only below 700 Hz or only above 2000 Hz may be rejected by the LIGO frequency selection, it is appropriate to say that the search is done in the 700-2000 Hz band. Further reduction in the false alarm rate could be achieved by restricting the TAMA frequency mask to 700-2000 Hz to match the frequency content of the LIGO triggers used in this analysis.

B. Coincidence and background

To minimize the possibility of falsely claiming a gravitational-wave detection, we require any candidate GWB to be observed simultaneously by all operating detectors. In this section we explain how the coincidence test was imposed, and how the background rate was estimated.

1. Coincidence

The coincidence test is very simple. Each event i is characterized by a peak time t_i and a duration Δt_i. Events from two detectors are defined to be in coincidence if the difference in their peak times satisfies

$$|t_i - t_j| < w + \tfrac{1}{2}(\Delta t_i + \Delta t_j). \tag{3.1}$$

Here w is a coincidence "window" which accounts for the light travel time between the detectors in question, and for the timing accuracy of our search algorithms. The duration-dependent term allows for the estimated peak time of coincident triggers to be farther apart if the triggers are long compared to the coincidence window; one may consider this as an another allowance for the uncertainty in the determination of the peak time. A set of event triggers $i, j, \ldots, k$ is defined to be in coincidence if each pair (i, j), (i, k), (j, k), etc., is in coincidence.

Ideally, the window w for each pair of detectors should be as short as possible, to minimize the rate of accidental coincidences between noise events in the various detectors, while still being long enough that all simulated signals detected are in coincidence. The windows for our analysis are determined using the simulations described in Sec. IV B.

It is observed that triggers in the S2 and DT8 data tend to be produced in clusters, on time scales of order 1 s or less. We therefore count groups of coincident triggers that are separated in time by less than 200 ms as a single coincidence when estimating rates. This clustering is done both for time-shifted and non-time-shifted coincidences. The coincidence rate after clustering does not depend strongly on the time scale used.

Note that no attempt is made to compare the amplitude or SNR of events between detectors. Such comparisons are difficult due to the differences in alignment of the detectors (except for the H1-H2 pair); see Fig. 1. We do, however, impose a test on the consistency of the waveform shape as measured by the various LIGO detectors; see Sec. III C.

2. Background

Even in the absence of real gravitational-wave signals, one expects some coincidences between random noise-generated events. We estimate this background rate by repeating the coincidence procedure after adding artificial relative time shifts of $\pm 5, 10, \ldots, 115$ s to the triggers from the LIGO Hanford and/or TAMA sites, as indicated in Fig. 4. (We do not shift the triggers from H1 and H2 relative to each other, in case there are true correlated noise coincidences caused by local environmental effects.) These shifts are much longer than the light travel time between the sites, so that any resulting coincidence cannot be from an actual gravitational wave. They are also longer than detector noise autocorrelation times (see Fig. 5), and shorter than time scales on which trigger rates vary, so that each provides an independent estimate of the accidental coincidence rate.

The H1-H2-nL1-T1 and H1-H2-L1-nT1 data sets each come from 2 sites, so that we have 46 nonzero relative time shifts in $\{-115, -110, \ldots, 115\}$ s. Hence, the smallest nonzero background rate that can be measured for these data sets is approximately $(46T_{2-\text{site}})^{-1}$, where $T_{2-\text{site}}$ is the observation time [27]. The H1-H2-L1-T1 network has

3 sites, for a total of $47^2 - 1 = 2208$ independent time shifts. We use all of these time shifts, so the smallest nonzero background rate that we can measure for the quadruple-coincidence data set is approximately $(2208T_{3-\text{site}})^{-1}$.

C. Waveform consistency test

The event generation and coincidence procedures outlined above are designed to detect simultaneous excesses of power in each detector, without regard to the waveform of the event. To test if the waveforms as measured in each detector are consistent with one another (as one would expect for a GWB), we apply a test based on the linear correlation coefficient between data streams, the r-statistic [28]. We will see in Sec. IV B that the r-statistic test is very effective at eliminating accidental coincidences, with very little probability of rejecting a true gravitational-wave signal. (See also [16] for demonstrations of the r-statistic with other simulated GWB waveforms.)

The r-statistic test consists of computing the cross-correlation of the time-series data from pairs of detectors around the time of a coincidence. A GWB will increase the magnitude of the cross-correlation above that expected from noise alone. The measured cross-correlations are compared to those expected from Gaussian noise using a Kolmogorov-Smirnov test with 95% confidence level. If not consistent, then the logarithmic significance (negative log of the probability) of each cross-correlation is computed and averaged over detector pairs. We refer to the resulting quantity as Γ. If the maximum averaged significance exceeds a threshold Γ_0, then the coincidence is accepted as a candidate GWB; otherwise it is discarded. The threshold Γ_0 is chosen sufficiently high to reduce the background by the desired amount without rejecting too many real GWB signals. For more details on the test, see [28].

The r-statistic test was developed for use in LIGO searches, and it is based on the premise that a real gravitational-wave signal will have similar form in different detectors. It is not clear that it can be applied safely to detectors with very different orientations (such as LIGO and TAMA), which see different combinations of the two polarizations of a gravitational wave. Since this matter is still under study, we use the r-statistic test to compare data between the LIGO detectors only (i.e., H1-H2, H2-L1, and L1-H1, but not including T1).

D. Statistical analysis

Our scientific goal of this search is to detect GWBs, or in the absence of detectable signals, to set an upper limit on their mean rate, and to estimate the minimum signal amplitude to which our network is sensitive.

The coincidence procedure described in Sec. III B produces two sets of coincident events. The set with no artificial time shift is produced by background noise and
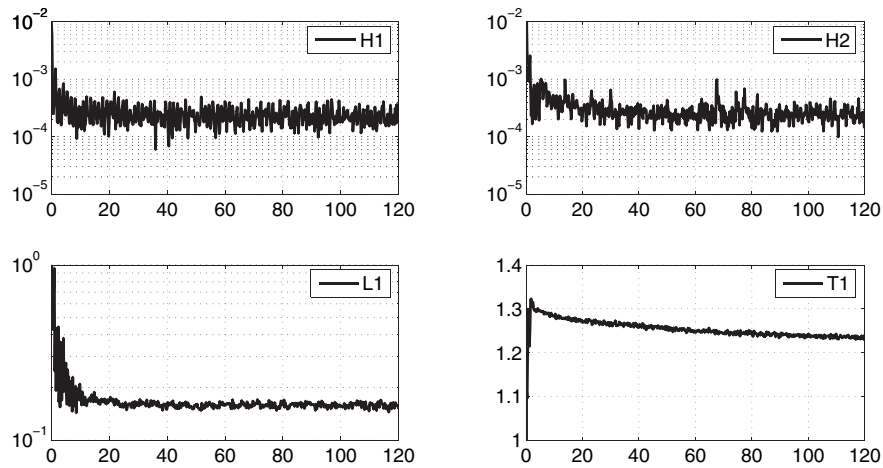
FIG. 5.   Autocorrelogram of trigger peak times from each detector. These are histograms of the difference in peak time between each pair of triggers from a given detector, binned in 0.2 s intervals. The horizontal axis is the time difference (units of s); the vertical axis is the number of trigger pairs per bin divided by the observation time and the bin width (units of s^{-2}). With this normalization, the mean value is the square of the trigger rate. An autocorrelogram value significantly above the mean indicates a correlation in the time of event triggers. Each detector shows some excess above Poisson rates at delays of up to a few seconds. The sharp dip in the T1 curve near zero time is due to the clustering of the T1 triggers. The smaller relative fluctuations in the L1 and T1 curves are due to the much higher trigger rates from these detectors, which results in more triggers per bin.

possibly also by gravitational-wave bursts. The time-shifted set contains only events produced by noise, and hence characterizes the background.

Given the number of candidate GWBs and the estimate of the number of accidental coincidences expected from the background, we use the Feldman-Cousins technique [29] to compute the 90% confidence level upper limit or confidence interval on the rate of detectable gravitational-wave bursts. In practice, since we are not prepared to claim a detection based purely on a blind statistical analysis, we choose in advance to use only the upper value of the Feldman-Cousins confidence interval. We report this upper value $R_{90\%}$ as an upper limit on the GWB rate, regardless of whether the Feldman-Cousins confidence interval is consistent with a rate of zero. Because of this modification our upper limit procedure has a confidence level greater than 90%; i.e., our upper limits are conservative.

The rate upper limit $R_{90\%}$ from the Feldman-Cousins procedure applies to GWBs for which our network has perfect detection efficiency. For a population of GWB sources for which our detection efficiency is $\epsilon(h)$, where h is the GWB amplitude and $0 \leq \epsilon(h) \leq 1$, the corresponding rate upper limit $R_{90\%}(h)$ is

$$R_{90\%}(h) \leq \frac{R_{90\%}}{\epsilon(h)}. \qquad (3.2)$$

This defines a region of rate-versus-strength space which is excluded at 90% confidence by our analysis. The exact domain depends on the signal type through our efficiency $\epsilon(h)$. We will construct such exclusion regions for one hypothetical population of GWB sources.

Note that our choice to present an upper limit on the GWB rate does not preclude also claiming a detection if a coincident signal is seen. It merely reflects that a candidate detection would be subjected to additional follow-up tests not included in our blind analysis. Such tests may include looking for potential environmental causes, or trying to determine a consistent GWB waveform that correlates well with the output of the individual detectors [15,30]. Such ''nonblind'' post-hoc tests are difficult to quantify in a frequentist upper limit (see [16] for an example). We therefore distinguish between setting upper limits and claiming detections of GWBs.

IV. SIMULATIONS AND TUNING

There are a number of parameters in the analysis pipeline of Fig. 4 that can be manipulated to adjust the sensitivity and background rate of our network. The most important are the thresholds for trigger generation (the TFCLUSTERS black-pixel probability p and the EXCESS POWER SNR threshold ρ_0), the r-statistic threshold Γ_0, and the coincidence windows w for each detector pair. Our strategy is to tune these parameters to maximize the sensitivity of the network to millisecond-duration signals while maintaining a background of less than 0.1 surviving coincidences expected over the entire S2/DT8 data set.

A. Simulations

The LIGO-TAMA network consists of widely separated detectors with dissimilar noise spectra and antenna responses. To estimate the sensitivity of this heterogeneous network we add (or ''inject'') simulated gravitational-wave

signals into the data streams from each detector, and reanalyze the data in exactly the same manner as is done in the actual gravitational-wave search; this is indicated in Fig. 4 by the "simulated signals" box. These injections are done coherently; i.e., they correspond to a GWB incident from a specific direction on the sky. The simulated signals include the effects of the antenna response of the detectors, and the appropriate time delays due to the physical separation of the detectors.

These simulations require that we specify a target population, including the waveform and the distribution of sources over the sky. We select a family of simple waveforms that have millisecond durations and that span the frequency range of interest, 700-2000 Hz. Specifically, we use linearly polarized Gaussian-modulated sinusoids:

$$h_+(t) = h_{\mathrm{rss}} \left(\frac{\pi}{2f_0^2} \right)^{-1/4} \sin[2\pi f_0(t - t_0)] \mathrm{e}^{-(t-t_0)^2/\tau^2},$$
$$h_\times(t) = 0. \qquad (4.1)$$

(Other waveforms, along with these, have been considered in [16,17,21].) Here t_0 is the peak time of the signal envelope. The central frequency f_0 of each injection is picked randomly from the values 700, 849, 1053, 1304, 1615, 2000 Hz, which span our analysis band in logarithmic steps. The efficiency of detection of these signals thus gives us a measure of the network sensitivity averaged over our band. We set the envelope width as $\tau = 2/f_0$, which gives durations of approximately 1-3 ms. The corresponding quality factor is $Q \equiv \sqrt{2}\pi f_0 \tau = 8.9$ and the bandwidth is $\Delta f = f_0/Q \simeq 0.1f_0$, so these are narrow-band signals.

The quantity h_{rss} in Eq. (4.1) is the root-sum-square amplitude of the plus polarization:

$$\left[\int_{-\infty}^{\infty} dt h_+^2(t) \right]^{1/2} = h_{\mathrm{rss}} \qquad (4.2)$$

We find h_{rss} to be a convenient measure of the signal strength. While it is a detector-independent amplitude, h_{rss} has the same units as the strain noise amplitude spectrum of the detectors, which allows for a direct comparison of the signal amplitude relative to the detector noise. All amplitudes quoted in this report are h_{rss} amplitudes.

Lacking any strong theoretical bias for probable sky positions of sources of short-duration bursts, we distribute the simulated signals isotropically over the sky. We select the polarization angle randomly with uniform distribution over $[0, \pi]$.

A total of approximately 16 800 of these signals were injected into the S2/DT8 data. For each signal, the actual waveform $h(t)$ as it would be seen by a given detector was computed,

$$h(t) = F^+ h_+(t) + F^\times h_\times(t) = F^+ h_+(t), \qquad (4.3)$$

and $h(t)$ was added to the detector data. Here F^+, $F^\times$ are the usual antenna response factors, which are functions of

the sky direction and polarization of the signal relative to the detector (see for example [19]). The signals in the different detectors were also delayed relative to one another according to the sky position of the source.

These simulated signals were shared between LIGO and TAMA by writing the signals $h(t)$ in frame files [31,32], including the appropriate detector response and calibration effects. These signal data were added to the data streams from the individual detectors before passing through TFCLUSTERS or EXCESS POWER. In addition to providing estimates of the network detection efficiency, the ability of these two independent search codes to recover the injected signals is an important test of the validity of the pipeline.

An injected signal is considered detected if there is a coincident event from the network within 200 ms of the injection time. The network efficiency $\epsilon(h_{\mathrm{rss}})$ is simply the fraction of events of amplitude h_{rss} which are detected by the network. We find that good empirical fits to the measured efficiencies can be found in the form

$$\epsilon(h_{\mathrm{rss}}) = \frac{1}{1 + \left(\frac{h_{\mathrm{rss}}}{h_{\mathrm{rss}}^{50\%}}\right)^{\alpha[1+\beta \tanh(h_{\mathrm{rss}}/h_{\mathrm{rss}}^{50\%})]}}, \qquad (4.4)$$

where $h_{\mathrm{rss}}^{50\%} > 0$, $\alpha < 0$, and $-1 < \beta \leq 0$. Here $h_{\mathrm{rss}}^{50\%}$ is the amplitude at which the efficiency is 0.5, α parametrizes the width of the transition region, and β parametrizes the asymmetry of the efficiency curve about $h_{\mathrm{rss}} = h_{\mathrm{rss}}^{50\%}$. When presenting efficiencies we will use fits of this type.

As we shall see, the efficiency transitions from zero (for weak signals) to unity (for strong signals), over about an order of magnitude in signal amplitude. It proves convenient to characterize the network sensitivity by the single number $h_{\mathrm{rss}}^{50\%}$ at which the efficiency is 0.5. This amplitude is a function of the trigger-generation thresholds; it and the background rate are the two performance measures that we use to guide the tuning of our analysis.

B. Tuning procedure

As stated earlier, our tuning strategy is to maximize the detection efficiency of the network while maintaining a background rate of less than approximately 0.1 events over the entire data set. For simplicity, we chose a single tuning for the production and analysis of all event triggers from all data sets. This strategy is implemented as follows:

(1) For TFCLUSTERS, the efficiency for detecting the sine-Gaussian signals and the background rate is measured for each detector for a large number of parameter choices. For each black-pixel probability p (which determines the background rate) the other ETG parameters are set to obtain the lowest $h_{\mathrm{rss}}^{50\%}$ value [33]. The TAMA EXCESS POWER algorithm is tuned independently for short-duration signals as described in [17]. The resulting performance of each detector is shown in Fig. 6.

(2) The coincidence window w for each detector pair in Eq. (3.1) is fixed by performing coincidence on the
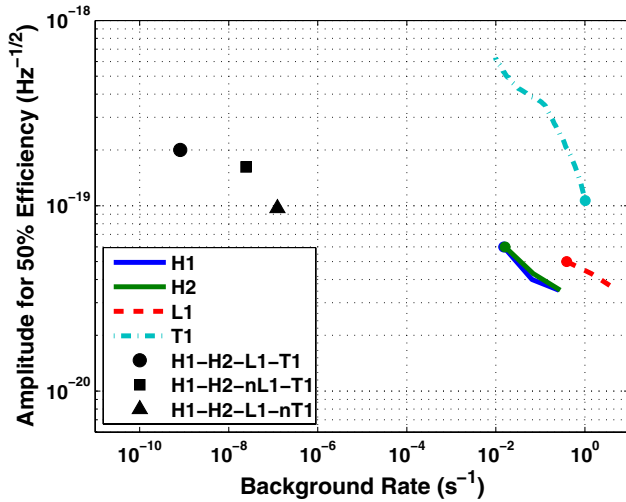
FIG. 6 (color online). Amplitude $h_{rss}^{50\%}$ for 50% detection efficiency versus background rate for each of the individual detectors, and for the three coincidence combinations. The circles on the single-detector curves indicate the tuning selected for trigger generation. The circle, square, and triangle denote the resulting amplitude at 50% efficiency and an upper limit on the background rate for the H1-H2-L1-T1, H1-H2-nL1-T1, and H1-H2-L1-nT1 networks after the r-statistic with these tuning choices. (We can only compute upper limits on the background rates for coincidence because no time-shifted coincidences survive the waveform consistency test.) The efficiency is averaged over all of the sine-Gaussian signals in our analysis band.

triggers from the simulated signals. We find the timing accuracy of TFCLUSTERS and EXCESS POWER to these simulated signals to be of order 1 ms. In practice, selecting windows only slightly larger (by ~1 ms) than the light travel time between the various detector pairs (see Table II) ensures that all of the injections detected by all interferometers produce coincident triggers. However, considering that our simulation population is restricted to signals of a single waveform type (Gaussian-modulated sinusoids) with durations of order 5 ms or less, we consider it prudent to allow for the possibility of larger timing error for other types of signals. For simplicity, we use a single window of $w = 20$ ms for coincidence between any LIGO detectors [34] and a single window of $w = 43$ ms for coincidence between any LIGO detector and TAMA. These

TABLE II. Separation of the LIGO and TAMA interferometers, using data from [19].

Detector pair	Separation (km)	Separation (ms)
LHO-LLO	3002	10.0
LLO-TAMA	9683	32.3
TAMA-LHO	7473	24.9

choices correspond to using the longest possible time delay plus a ~10 ms safety margin.

(3) To obtain the best network sensitivity versus background rate, we select the single-detector ETG thresholds (p, ρ_0) to match $h_{rss}^{50\%}$ as closely as possible between the detectors. (This is similar in spirit to the IGEC tuning [7], although not the same, as we are not able to easily compare the amplitude of individual events from our misaligned broadband detectors.) In practice, the TAMA detector has slightly poorer sensitivity than the LIGO detectors. We therefore set the TAMA threshold as low as we consider feasible, $\rho_0 = 4$; this sets the sensitivity of the network as a whole. We then choose the LIGO single-detector thresholds for similar efficiency.

(4) The final threshold is that for the r-statistic, Γ_0. In practice we find that the r-statistic has negligible effect on the network efficiency for $\Gamma_0 < 5$. We set $\Gamma_0 = 3$, which proved sufficient to eliminate all time-lagged (accidental) coincidences. With this threshold the r-statistic rejects less than 1% of the signals detected by TFCLUSTERS. All of the rejected signals are of relatively low amplitude. Figure 6 shows the resulting $h_{rss}^{50\%}$ and background rate for each of the three coincidence combinations. Table III shows trigger rates and livetimes for each coincidence combination.

We note from Fig. 6 that the network background rates are 5–9 orders of magnitude smaller than the rates of the individual detectors. Roughly speaking, adding a detector with event rate R_i and coincidence window w to the network changes the network background rate by a factor of approximately $2R_i w$. From the single-detector rates of Fig. 6 or Table III we estimate that H1 and H2 each reduce the background rate by ~10^3, L1 by ~50, and T1 by ~10. This is why we require both H1 and H2 to be operating: they suppress strongly the background for our network.

We have confirmed that the background rate estimated from time shifts is consistent with that expected from Poisson statistics. Assuming Poisson statistics, the expected background rate R for a set of N detectors with rates R_i is approximately

$$R \approx \frac{1}{w} \prod_{i=1}^{N} 2R_i w \qquad (4.5)$$

where we assume a single coincidence window w for simplicity [35]. Using this formula and the single-detector rates from Table III, one predicts background rates before the r-statistic consistent with those determined from time delays. This agreement gives increased confidence in our background estimation.

It is also worth noting that the 50% efficiency point $h_{rss}^{50\%}$ is a very shallow function of the background rate for multiple detectors. Hence, there is little value in lowering

TABLE III. Results of the LIGO-TAMA analysis for each data set separately, and combined. R_{H1}, etc., are the measured single-detector trigger rates. N is the total number of coincidences before/after the r-statistic waveform consistency test. T is the total observation time analyzed, after removal of the playground and veto dead times. N_{bck} and T_{bck} are the corresponding summed numbers from the time-shift experiments. $\langle N \rangle$ is the expected number of accidental coincidences during the observation time. (For $N_{bck} = 0$, we estimate $\langle N \rangle < T/T_{bck}$.) $R_{90\%}$ is the resulting upper limit on the rate of detectable gravitational-wave events, at 90% confidence.

Data Set	H1-H2-L1-T1	H1-H2-nL1-T1	H1-H2-L1-nT1	Combined
R_{H1} (s^{-1})	0.0157	0.0151	0.0137	$\cdots$
R_{H2} (s^{-1})	0.0164	0.0183	0.0150	$\cdots$
R_{L1} (s^{-1})	0.399	$\cdots$	0.377	$\cdots$
R_{T1} (s^{-1})	1.03	1.04	$\cdots$	$\cdots$
N	0/0	1/0	0/0	1/0
T (hr)	165.3	257.0	51.2	473.5
N_{bck}	31/0	57/0	0/0	$\cdots$
T_{bck} (hr)	3.422×10^5	1.139×10^4	2.243×10^3	$\cdots$
$\langle N \rangle$	0.015/ < 0.0005	1.3/ < 0.03	<0.03/ < 0.03	<1.4/ < 0.05
$R_{90\%}$ (day^{-1})	0.35	0.23	1.1	0.12

the trigger thresholds to attempt to detect weaker signals. For example, allowing the triple-coincidence background rate of TFCLUSTERS (the rate for the H1-H2-L1-nT1 data) to increase by 3 orders of magnitude lowers $h_{rss}^{50\%}$ by less than a factor of 2. For four detectors, $h_{rss}^{50\%}$ varies even more slowly with the background rate. This is why we tune for $\ll 1$ background event over the observation time; there is almost no loss of efficiency in doing so.

To avoid bias from tuning our pipeline using the same data from which we derive our upper limits, the tuning was done without examining the full zero-time-shift coincidence trigger sets. Instead, preliminary tuning was done using a 10% subset of the data, referred to as the *playground*, which was not used for setting upper limits. Final tuning choices were made by examining the time-shifted coincidences and the simulations over the full data set. As it happens, the only parameter adjusted in this final tuning was the r-statistic threshold Γ_0; we required the full observation time to have enough background coincidences to allow reasonably accurate estimates of the background suppression by the r-statistic test.

Figure 7 shows the efficiency of the LIGO-TAMA network as a function of signal amplitude for each of the three
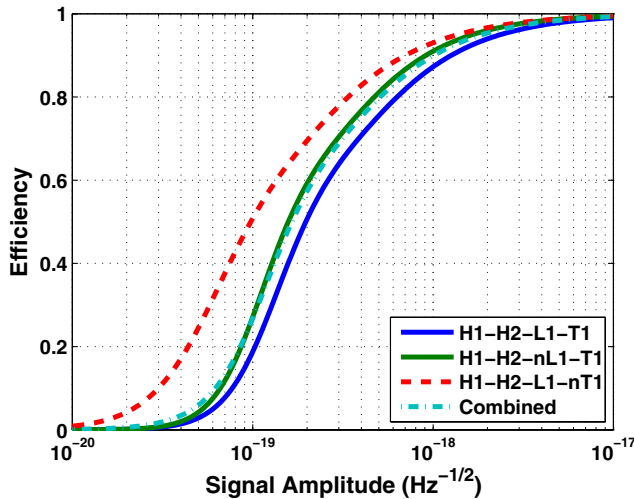

FIG. 7 (color online). Detection efficiency over the various data sets individually, and combined, using the final tuning. The combined efficiency curve is the average of the curves for the three data sets, weighted by their observation times. These efficiencies are averaged over all of the sine-Gaussian signals in our analysis band. There is a statistical uncertainty at each point in these curves of approximately 1%–3% due to the finite number of simulations performed.
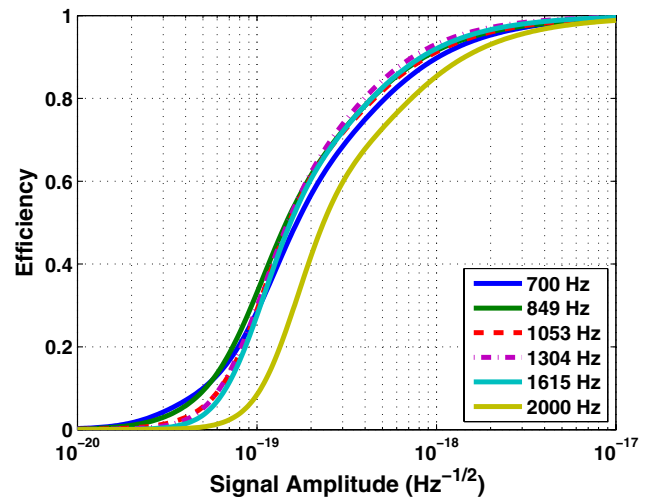

FIG. 8 (color online). Detection efficiency for the combined data set, by central frequency f_0 of the sine-Gaussian signal in Eq. (4.1). There is a statistical uncertainty at each point in these curves of approximately 2%–4% due to the finite number of simulations performed.
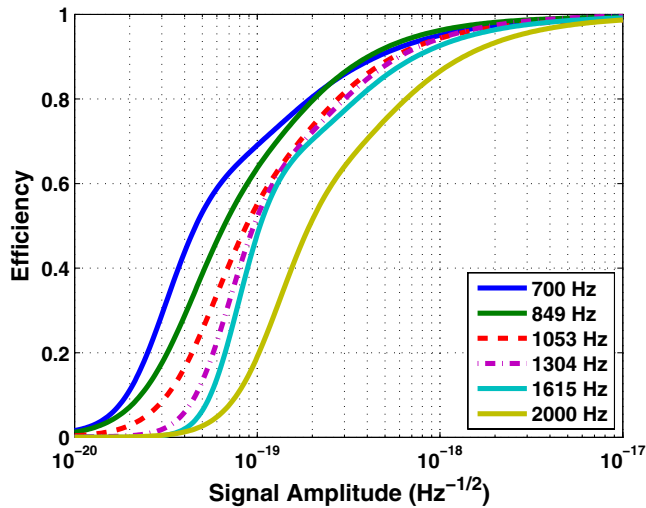
FIG. 9 (color online). Detection efficiency for the H1-H2-L1-nT1 data set (i.e., with only the LIGO detectors operating), by central frequency f_0 of the sine-Gaussian signal in Eq. (4.1). There is a statistical uncertainty at each point in these curves of approximately 2%–6% due to the finite number of simulations performed. The improved efficiency for lower-frequency signals indicates that sensitivity at these frequencies is limited by the TAMA detector. This behavior is consistent with the noise spectra shown in Fig. 3.

data sets, and also the average efficiency weighted by the observation time of each data set. By design, the efficiencies are very similar, with $h_{\text{rss}}^{50\%}$ values in the range 1–2×10^{-19} Hz$^{-1/2}$.

Figure 8 shows how the combined efficiency varies across our frequency band; the weak dependence on the central frequency of the injected signal is a consequence of the flatness of the envelope of the detector noise spectra shown in Fig. 3. This is corroborated by the efficiency for the H1-H2-L1-nT1 data set (without TAMA), shown in Fig. 9. The improvement in the low-frequency sensitivity for this data set indicates that TAMA limits the network sensitivity at low frequencies, as expected from the noise spectra.

C. Systematic and statistical uncertainties

The only significant systematic uncertainty in our analysis is in the overall multiplicative scale of the calibration (the coupling of strain to the output of the individual detectors). The "1-σ" uncertainties were estimated as $\sim 9\%$ for L1 and $\sim 4\%$ for each of H1, H2, and T1 [36]. Simple Monte-Carlo modeling indicates that, with 90% confidence, the $h_{\text{rss}}^{50\%}$ value for any given network combination will not be more than 4% larger than the estimated value due to these uncertainties. We allow for this uncertainty in our rate-versus-strength plots by shifting our limit curves to larger h_{rss} by 4%.

The main statistical uncertainty in our results is in the efficiency at any given signal amplitude, due to the finite

number of simulations performed. This can be quantified through the uncertainty in the parameters found for the efficiency fits (4.4), and is typically less than 5%. We account for this by shifting our rate-versus-strength upper limit curves upward at each amplitude by 1.28 times the estimated statistical uncertainty in the corresponding efficiency. (The factor 1.28 gives a 90% limit, assuming Gaussian statistics.)

V. ANALYSIS RESULTS

After making the final tuning choices, we performed the coincidence analysis without time shifts for all three data sets. No event triggers survived the coincidence and r-statistic tests, so we have no candidate gravitational-wave signals.

Table III shows for each data set the rate of triggers, the number of coincident events before and after the r-statistic test, and the total amount of data analyzed after removing the playground and accounting for the dead time of the TAMA vetoes. Also shown are the number of accidental coincidences and the effective observation time from the time-shift experiments, which provide our estimate of the background rates. Finally, the upper limits on the rate of detectable gravitational-wave bursts are shown.

As discussed in Sec. III D, our upper limits are obtained using the Feldman-Cousins procedure [29]. This algorithm compares the observed number of events to that expected from the background. From Table IV of [29], one finds that for a fixed number of observed events, the Feldman-Cousins upper limit is stronger (lower) for higher backgrounds. Since our backgrounds are too low to be measured accurately (there are no surviving time-shifted coincidences after the r-statistic), we conservatively assume zero background in calculating our upper limits. Since there are also no surviving coincidences without time shifts, the rate limits from the Feldman-Cousins procedure take on the simple form

$$R_{90\%}^i = \frac{2.44}{T_i} \tag{5.1}$$

where T_i is the observation time for a particular network combination (see Table IV of [29] with $b = 0$, $n = 0$). This gives the limits shown in Table III. Additionally, since all three data sets have essentially zero background, we can treat them collectively as a single experiment by summing their observation times and the number of detected events (which happens to be zero):

$$R_{90\%}^{\text{combined}} = \frac{2.44}{\sum_i T_i} \tag{5.2}$$

The resulting upper limit of 0.12 detectable events per day at 90% confidence is the primary scientific result of this analysis.
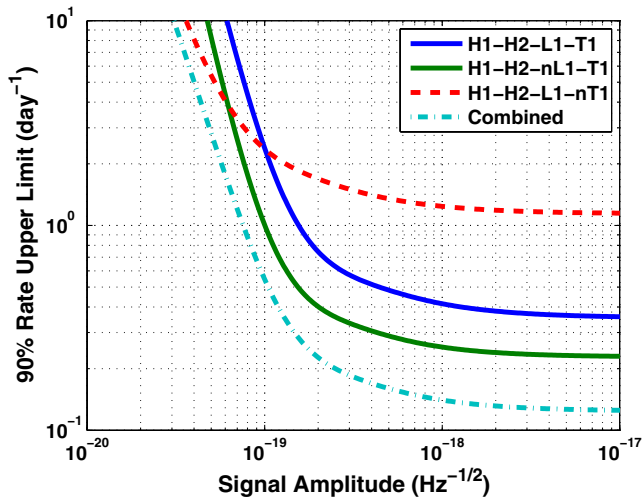
FIG. 10 (color online). Rate-versus-strength upper limits from each LIGO-TAMA data set, and combined, for the isotropic distribution of sources of sine-Gaussian GWBs described in Sec. IV A. The region above any curve is excluded by that experiment with at least 90% confidence. These curves include the allowances for uncertainties in the calibration and in the efficiencies discussed in Sec. IV C.

By dividing the rate upper limits by the efficiency for a given population of GWB sources, as in Eq. (3.2), we obtain upper limits on the GWB rate as a function of the burst amplitude. Averaging over the network combinations gives

$$R_{90\%}^{\text{combined}}(h_{\text{rss}}) = \frac{2.44}{\sum_i \epsilon_i(h_{\text{rss}})T_i} \tag{5.3}$$

For example, for our tuning population of isotropically distributed sources of sine-Gaussian GWBs, and averaging over all f_0 (i.e., using the efficiencies in Fig. 7), one obtains the rate-versus-strength upper limits shown in Fig. 10. GWB rates and amplitudes above a given curve are excluded by that data set with at least 90% confidence.

A. Comparison to other searches

The LIGO-TAMA search for GWBs is one of several such searches reported recently. Table IV shows the ob-

TABLE IV. Observation times, rate upper limits, and frequency bands for LIGO-TAMA and other recent burst searches [7,16,17]. The stated frequency range for the IGEC search is the range of the resonant frequencies of the detectors used. The IGEC upper limit applies only to signals with significant power at the resonant frequencies of all of the operating detectors.

Network	T (day)	$R_{90\%}$ (day^{-1})	band (Hz)
LIGO-TAMA S2/DT8	19.7	0.12	700-2000
LIGO-only S2	10.0	0.26	100-1100
TAMA-only DT9	8.1	0.49	230-2500
IGEC	707.9	0.0041	694-930

servation time, rate upper limit, and approximate frequency band for LIGO-TAMA, the LIGO-only S2 search [16], the TAMA-only DT9 search [17], and the IGEC search [7]. Our limit of 0.12 events per day is the strongest limit yet placed on gravitational-wave bursts by broadband detectors. Even so, it is still approximately a factor of 30 larger than the IGEC limit, which was derived from approximately two years of data from a network of 5 resonant-mass detectors. Note however that the broadband nature of the LIGO and TAMA detectors means that they are sensitive to a wider class of signals than resonant-mass detectors; the IGEC search is only sensitive to GWBs with significant power at the resonant frequencies of all of the operating detectors.

Since our sine-Gaussian test waveforms are narrow-band signals, we cannot compare directly our sensitivity to that of the IGEC network. More concrete comparisons can be made between the performance of the LIGO-TAMA network and LIGO and TAMA individually, by considering the rate-versus-strength upper limit for $f_0 = 849$ Hz sine-Gaussians. Figure 11 shows the upper limits for this waveform from the LIGO-only S1 and S2 searches [16,21], the TAMA DT9 search [17], and the present analysis. Compared to LIGO alone, the much longer observation time afforded by joining the LIGO and TAMA detectors allows the LIGO-TAMA network to set stronger rate upper
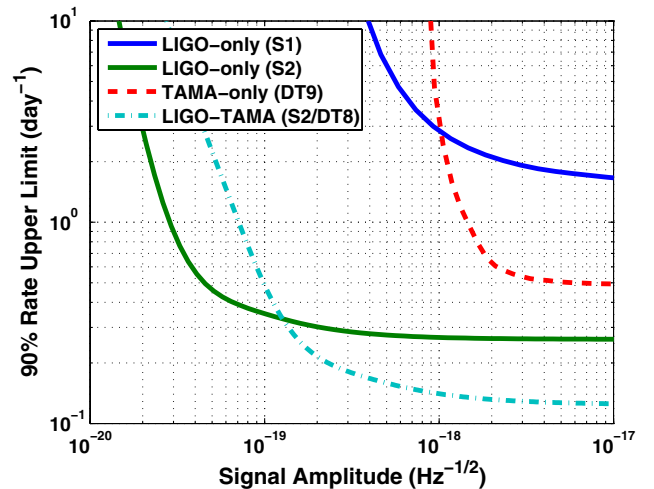

FIG. 11 (color online). Comparison of the rate-versus-strength upper limits for $f_0 = 849$ Hz sine-Gaussians from the combined LIGO-TAMA data set (including systematic and statistical uncertainties) with those from the LIGO-only S1 and S2 bursts searches [16,21] and the TAMA-only DT9 search [17]. The combined LIGO-TAMA network has a superior rate upper limit for strong signals due to its larger observation time, while the LIGO-only S2 network has better sensitivity to weak signals. The TAMA-only DT9 amplitude sensitivity is limited by the high SNR threshold needed achieve a background rate of order one event over the observation time. Note that the LIGO-only S2 search had a nominal frequency range of 100-1100 Hz, while the LIGO-TAMA search band is 700-2000 Hz.

limits for amplitudes at which both LIGO and TAMA are sensitive. The joint network also enjoys a lower background rate from accidental coincidences, particularly for the quadruple-coincidence network: of order $1/40$ yr^{-1} for quadruple coincidence, versus of order 2 yr^{-1} for the LIGO-only S2 analysis. However, the band of good sensitivity for LIGO-TAMA does not extend to low frequencies, due to the poorer TAMA noise level there. The LIGO-only analysis also has better sensitivity to weak signals, especially near the lower edge of our frequency band. Compared to TAMA alone, the LIGO-TAMA network has better sensitivity to weak signals because coincidence with LIGO lowers the network background rate without requiring high thresholds for trigger generation. For example, while the TAMA noise levels were lower in DT9 than in DT8, the TAMA DT9 amplitude sensitivity is not as good as that of LIGO-TAMA due to the need to use a very high SNR threshold—$\rho_0 = 10^4$—to reduce the TAMA-only background rate to of order one event over the observation time.

VI. CONCLUSION

The LIGO and TAMA collaborations have completed their first joint search for gravitational-wave bursts, using 473 hr of coincident data collected during early 2003. We looked for millisecond-duration gravitational-wave bursts in the frequency range 700-2000 Hz, where all four of the detectors had comparable sensitivity. To maintain a low background, we analyzed data only from periods when at least three interferometers (including the two LIGO-Hanford interferometers) were operating, and we required candidate signals to be observed simultaneously in all of the operating detectors. We used coordinated injections of simulated gravitational-wave signals to estimate the detection efficiency of our heterogeneous network. We matched the efficiency between detectors to maximize the network sensitivity while limiting the background rate to less than 0.1 events expected over the entire observation time. No gravitational-wave candidates were observed, and we place an upper bound of 0.12 events per day on the rate of detectable millisecond-duration gravitational-wave bursts with at least 90% confidence. Simulations indicate that our network has a detection efficiency of at least 50% (90%) for narrow-band signals with root-sum-square strain amplitude greater than approximately 2×10^{-19} Hz$^{-1/2}$ (10^{-18} Hz$^{-1/2}$) in the frequency band 700-2000 Hz.

This analysis highlights both advantages and disadvantages of joint coincidence searches compared to independent searches by LIGO and TAMA. Together, the LIGO-TAMA network has more than twice as much data with three or more detectors in simultaneous operation than LIGO alone, leading to stronger rate limits. We also enjoy a background rate of order one event per 40 years (or lower) in quadruple-coincidence operation. The lower background from coincidence also allows the TAMA data to be analyzed with lower thresholds for signal detection. These benefits come at some cost in detection efficiency and in bandwidth, particularly at low frequencies. This is a result of requiring coincident detection by all interferometers, in which case the network sensitivity is limited by the least sensitive detector at each frequency.

This analysis may serve as a prototype for more comprehensive collaborative searches in the future. One improvement would be to expand the detector network. For example, GEO, LIGO, and TAMA performed coincident data taking during Oct. 2003–Jan. 2004; a GEO-LIGO-TAMA network would contain 5 interferometers at four sites, with excellent sky coverage. Another improvement would be to implement a fully coherent consistency test of coincident events, including all of the detectors in the network. For example, the Gursel-Tinto technique [15] would allow us to take advantage of the different detector orientations to try to extract sky direction and waveform information from detected gravitational-wave signals. It would also allow us to reject a coincidence if no consistent sky direction or waveform could be determined [30].

ACKNOWLEDGMENTS

[1] B. Willke *et al.*, Classical Quantum Gravity **21**, S417 (2004).

[2] D. Sigg, Classical Quantum Gravity **21**, S409 (2004).

[3] R. Takahashi, Classical Quantum Gravity **21**, S403 (2004).

[4] F. Acernese *et al.*, Classical Quantum Gravity **21**, S385 (2004).

[5] E. Amaldi *et al.*, Astron. Astrophys. **216**, 325 (1989).

[6] Z. A. Allen *et al.*, Phys. Rev. Lett. **85**, 5046 (2000).

[7] P. Astone *et al.*, Phys. Rev. D **68**, 022001 (2003).

[8] T. Zwerger and E. Muller, Astron. Astrophys. **320**, 209 (1997).

[9] M. Shibata and Y. I. Sekiguchi, Phys. Rev. D **69**, 084024 (2004).

[10] H. Dimmelmeier, J. Font, and E. Muller, Astron. Astrophys. **393**, 523 (2002).

[11] C. Ott, A. Burrows, E. Livne, and R. Walder, Astrophys. J. **600**, 834 (2004).

[12] É. É. Flanagan and S. A. Hughes, Phys. Rev. D **57**, 4535 (1998).

[13] É. É. Flanagan and S. A. Hughes, Phys. Rev. D **57**, 4566 (1998).

[14] P. Mészáros, Annu. Rev. Astron. Astrophys. **40**, 137 (2002).

[15] Y. Gursel and M. Tinto, Phys. Rev. D **40**, 3884 (1989).

[16] B. Abbott *et al.*, Phys. Rev. D **72**, 062001 (2005).

[17] M. Ando *et al.*, Phys. Rev. D **71**, 082002 (2005).

[18] W. Althouse *et al.*, Rev. Sci. Instrum. **72**, 3086 (2001).

[19] W. G. Anderson, P. R. Brady, J. D. E. Creighton, and É. É. Flanagan, Phys. Rev. D **63**, 042003 (2001).

[20] B. Abbott *et al.*, Nucl. Instrum. Methods Phys. Res., Sect. A **517**, 154 (2004).

[21] B. Abbott *et al.*, Phys. Rev. D **69**, 102001 (2004).

[22] V. Fafone, Classical Quantum Gravity **21**, S377 (2004).

[23] The LIGO software used in this analysis is available in the LIGO Scientific Collaboration's CVS archives at http://www.lsc-group.phys.uwm.edu/cgi-bin/cvs/viewcvs.cgi/?cvsroot=lscsoft; TFCLUSTERS is in LAL and LALWRAPPER, while the *r*-statistic and all other driver and post-processing codes are in the MATAPPS subsection. The version tag is RSTAT-1-2TAG for the *r*-statistic and S2LIGOTAMA 20050525 A for the other driver and post-processing codes. The TFCLUSTERS version is that for LDAS version 1.1.0; see http://www.ldas-sw.ligo.caltech.edu/ cgi-bin/index.cgi.

[24] J. Sylvestre, Phys. Rev. D **66**, 102004 (2002).

[25] S. Chatterji, L. Blackburn, G. Martin, and E. Katsavounidis, Classical Quantum Gravity **21**, S1809 (2004).

[26] The prefiltering for TFCLUSTERS was done in two stages. First, a sixth order modified butterworth high-pass filter with a cutoff frequency of 100 Hz was applied. Then a detector-dependent FIR linear predictor error filter was applied. The LPEF filters have approximately unity rms output, a training time of 4 seconds (from the middle of the lock segment being analyzed), and order of 1024.

[27] The smallest nonzero measurable rate is slightly higher than $(46T_{2-\mathrm{site}})^{-1}$ because triggers within 115 s of the edge of a data segment are dropped in some time shifts. The same holds for the 3-site time shifts.

[28] L. Cadonati, Classical Quantum Gravity **21**, S1695 (2004).

[29] G. J. Feldman and R. D. Cousins, Phys. Rev. D **57**, 3873 (1998).

[30] L. Wen and B. Schutz, Classical Quantum Gravity **22**, S1321 (2005).

[31] (LIGO Data and Computing Group and Virgo Data Acquisition Group), LIGO Report No. LIGO-T970130-F, 2002.

[32] S. Klimenko, M. Rakhmanov, and I. Yakushin, LIGO Report No. LIGO-T040042-00, 2004.

[33] In the notation of [24], the parameters used for TFCLUSTERS in this analysis are a segment length of 300 s, $\alpha = 1$, $\sigma = 2$, $\vec{\delta} = 0$ (no generalized clusters), $p = 10^{-4}$ (H1, H2), $p = 10^{-3}$ (L1), time resolution $T = 1/128$ s, $f_{\min} = 700$ Hz, $f_{\max} = 2000$ Hz. In contrast to [24], the black-pixel threshold is set by simply ranking the pixel powers, rather than by using a Rice fit.

[34] We could have imposed a tighter coincidence window between H1 and H2, since they are colocated, and further reduced the background rate. This is not necessary, however, since the false rate is already too small to be measured accurately; see Table III.

[35] The typical trigger durations are ~ 1 ms for LIGO and $\sim 5 - 8$ ms for TAMA. These are much less than the light travel times, so that the dominant contribution to the background comes from the window term w.

[36] G. González, M. Landry, B. O'Reilly, and H. Radkins, LIGO Report No. LIGO-T040060-01, 2004.